



HAL
open science

The Lomonosov Crater Impact Event: A Possible Mega-Tsunami Source on Mars

F. Costard, A. Séjourné, A. Lagain, J. Ormö, J.A.P. Rodriguez, S. Clifford, S.
Bouley, Karim Kelfoun, F. Lavigne

► **To cite this version:**

F. Costard, A. Séjourné, A. Lagain, J. Ormö, J.A.P. Rodriguez, et al.. The Lomonosov Crater Impact Event: A Possible Mega-Tsunami Source on Mars. *Journal of Geophysical Research. Planets*, 2019, 124 (7), pp.1840-1851. 10.1029/2019JE006008 . hal-02360771

HAL Id: hal-02360771

<https://hal.science/hal-02360771v1>

Submitted on 17 Nov 2020

HAL is a multi-disciplinary open access archive for the deposit and dissemination of scientific research documents, whether they are published or not. The documents may come from teaching and research institutions in France or abroad, or from public or private research centers.

L'archive ouverte pluridisciplinaire **HAL**, est destinée au dépôt et à la diffusion de documents scientifiques de niveau recherche, publiés ou non, émanant des établissements d'enseignement et de recherche français ou étrangers, des laboratoires publics ou privés.

RESEARCH ARTICLE

10.1029/2019JE006008

Key Points:

- Unusual morphometric characteristics of Lomonosov crater in comparison to the other northern complex craters
- Lomonosov crater was probably due to the presence of a shallow ocean of liquid water at the time of the impact
- Agreement of the Lomonosov age with that of the Thumbprint Terrain unit (~3 Ga) suggests that it was the source crater of the tsunami

Supporting Information:

- Supporting Information S1

Correspondence to:

F. Costard,
francois.costard@u-psud.fr

Citation:

Costard, F., Séjourné, A., Lagain, A., Ormö, J., Rodríguez, J. A. P., Clifford, S., et al. (2019). The Lomonosov crater impact event: A possible mega-tsunami source on Mars. *Journal of Geophysical Research: Planets*, 124, 1840–1851. <https://doi.org/10.1029/2019JE006008>

Received 19 APR 2019

Accepted 19 JUN 2019




Accepted article online 26 JUN 2019

Published online 12 JUL 2019

Author Contributions:

Data curation: A. Lagain**Funding acquisition:** F. Costard**Investigation:** F. Costard, J. Ormö, J. A.P. Rodriguez, K. Kelfoun, F. Lavigne**Methodology:** A. Séjourné, J. Ormö, J. A.P. Rodriguez, S. Bouley, K. Kelfoun**Resources:** A. Lagain**Supervision:** F. Costard**Writing - original draft:** F. Costard, A. Séjourné, A. Lagain, J. Ormö, J.A.P. Rodriguez, S. Clifford, S. Bouley

The Lomonosov Crater Impact Event: A Possible Mega-Tsunami Source on Mars

F. Costard¹ , A. Séjourné¹ , A. Lagain^{1,2} , J. Ormö³, J.A.P. Rodriguez⁴, S. Clifford⁴ , S. Bouley¹, K. Kelfoun⁵ , and F. Lavigne⁶

¹GEOPS-Géosciences Paris Sud, Université Paris-Sud, CNRS, Université Paris-Saclay, Orsay, France, ²School of Earth and Planetary Science, Curtin University, Perth, Western Australia, Australia, ³Astrobiology Centre, Instituto Nacional de Técnica Aeroespacial, Torrejón de Ardoz, Spain, ⁴Planetary Science Institute, Tucson, AZ, USA, ⁵Laboratoire Magmas et Volcans, OPGC, UBP-IRD-CNRS, Aubière, France, ⁶Université Paris 1, Panthéon-Sorbonne, Laboratoire de Géographie Physique, UMR 8591, Meudon, France

Abstract Recent research suggests that major meteorite impact events into a Late Hesperian/Early Amazonian ocean likely produced a mega-tsunami that would have resurfaced coastal areas in northwestern Arabia Terra. The orientations of the associated lobate deposits, a conspicuous type of landforms called Thumbprint Terrain, suggests that if an impact event triggered the mega-tsunami, the most likely location of the source crater is within the northern plains regions situated north of Arabia Terra. This study focuses on the identification of impact craters that impacted into the ocean and are likely to have produced the tsunami. We selected 10 complex impact craters, based on their diameters, location, and geomorphic characteristics. Of those, the Late Hesperian ~120-km-diameter Lomonosov crater exhibits a unique topographic plan view asymmetry (compared to other similar-sized and similar-aged craters in the northern plains such as Micoud, Korolev, and Milankovic). We attribute its broad and shallow rim, in part, to an impact into a shallow ocean as well as its subsequent erosion from the collapsing transient water cavity. The likely marine formation of the Lomonosov crater, and the apparent agreement in its age with that of the Thumbprint Terrain unit (~3 Ga), strongly suggests that it was the source crater of the tsunami. These results have implications for the stability of a late northern ocean on Mars.

1. Background

1.1. The Northern Plains of Mars and the Tsunami Hypothesis

The hypothesis that the northern plains may have been covered by a Late Hesperian/Early Amazonian ocean remains one of the most interesting, but also controversial, issues in Mars exploration. Geologic evidence of a putative northern ocean includes the identification of possible paleoshorelines at two elevations (Contacts 1 and 2, -3,760 and -3,940 m, respectively; Citron et al., 2018; Clifford & Parker, 2001; Parker et al., 1993, 1989, 1; Figure S1 in the supporting information. However, the identity (and continuity) of the proposed “shorelines” as water-related landforms has been questioned (Carr & Head, 2003; Ghatan & Zimelman, 2006; Malin & Edgett, 1999). Recently, Sholes et al. (2019) claim that the putative shoreline terraces do not follow an equipotential surface and are not laterally continuous. Finally, a long-lived ocean in the Late Hesperian/Early Amazonian is difficult to reconcile with existing climate models, which suggest that such an ocean would have frozen and sublimed away in a geologically short period of time (Turbet & Forget, 2019; Wordsworth, 2016).

Arabia Terra (centered at 45°N and 10°E) includes numerous examples of thumbprint terrains (TT) along its northern border, close to Contact 2 (see S1). That unit includes curvilinear ridges and hills with concentric lobes that are 10 to 20 m thick. They have been interpreted as mud volcanoes (Salvatore & Christensen, 2014; Tanaka et al., 2014), moraines or ice-cored ridges associated with a former glacial environment (Guidat et al., 2015; Lucchitta, 1981), but their exact origin is still debated. Rodriguez et al. (2016) and Costard et al. (2017) independently mapped the distribution of TT lobate deposits and found that they extend up to 150 km beyond the location of the proposed paleoshoreline, climbing local slopes and reaching elevations of over ~100 m. These lobate deposits exhibit features characteristic of terrestrial tsunami runup deposits, which suggests a similar origin (Costard et al., 2017; Rodriguez et al., 2016).

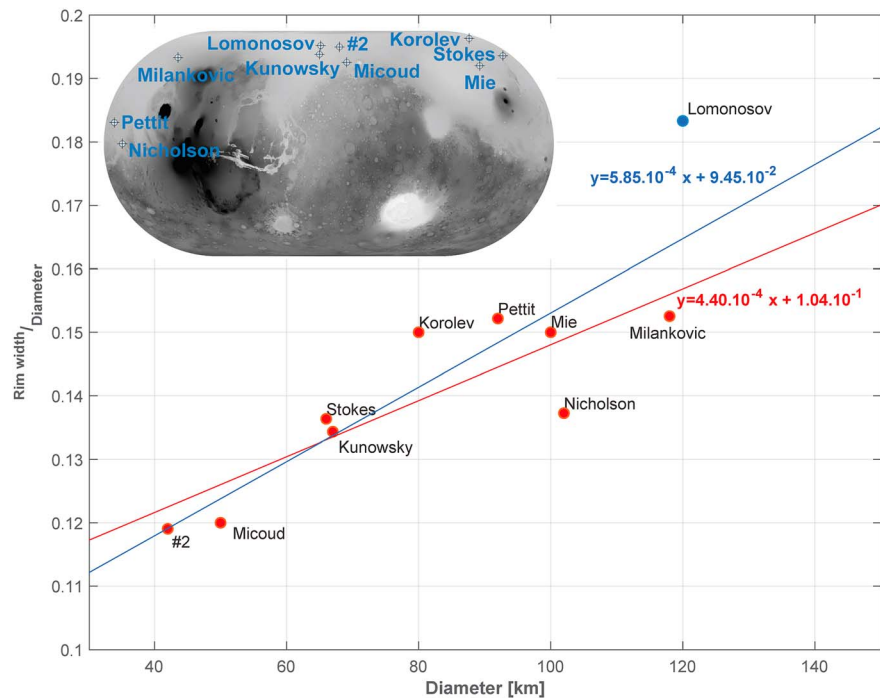


Figure 1. Comparative analysis of the normalized width of crater rims for different northern plains impact craters (see Table 1). Linear best fits are shown that both include and omit (in red) Lomonosov. Lomonosov appears distinct from other craters with diameters >100 km (Mie, Nicholson, and Milankovic) by having a relatively wider rim (normalized to crater diameter). Note that Lyot crater was not taken into account due to the fact that its diameter (250 km) places it in the peak ring crater category, so different from the complex crater morphology.

The orientations of the TT lobate deposits indicate that, if an impact event triggered the mega-tsunami, the source crater should be located to the north of the Highland-Lowland boundary in Arabia Terra. However, the identification of a marine target is complicated by the long and complex geological history of the northern plains (Tanaka et al., 2014). During the Late Hesperian, the Vastitas Borealis Formation covered most of the planet’s northern plains (Tanaka et al., 2014). This geologic unit consists of sedimentary material produced from multiple episodes of outflow channel discharge (e.g., Baker et al., 1991; Carr & Head, 2003; Clifford & Parker, 2001). Episodic reflooding of the northern plains by outflow channel activity may have persisted well into the Early Amazonian (Warner et al., 2009; Rodriguez et al., 2014, 2015). During the Late Amazonian, significant variations in Martian orbital parameters are thought to have induced cyclic accumulations of ice in different areas of the northern plains. Later, the high latitudinal regions of the northern plains were covered by an ice-rich and geologically young (0.4–2.1 Ma) latitude-dependent mantle that smoothed the topography (Head et al., 2003; Kreslavsky & Head, 2002; Mustard et al., 2001).

Table 1
Impact Craters Used in Our Morphometric Approach (See Figure 1)

Crater name	Latitude	Longitude	Crater diameter (km)	Rim width (km)
Lomonosov	64.9°N	9.2°W	120	22
Micoud	50.9°N	343.7°W	50	6
Crater #2	64°N	349°W	42	5
Milankovic	54.7°N	146.7°W	118	18
Korolev	73°N	195.5°W	80	12
Nicholson	0.2°N	163.6°W	105	15.5
Mie	48.5°N	220.4°W	100	15
Petit	12.39°N	173.87°W	95	14.5
Stokes	55.9°N	188.8°W	64	8.7
Kunowsky	57.1°N	9.7°W	66	8.9

In the absence of plate tectonics, it seems likely that Martian tsunamis would have been formed by large impacts into the proposed northern ocean (Ormö et al., 2004, 2002; Mahaney et al., 2010). Some potential marine impact source craters have been identified within areas encompassed by Contact 2, especially the “shelf” area of Arabia Terra (Ormö et al., 2004; Villiers et al., 2010), several of which were used as the basis for tsunami propagation simulations (Costard et al., 2017; Iijima et al., 2014; Matsui et al., 2001; Figure S1).

The numerical tsunami propagation models of Costard et al. (2017) suggested three potential source craters (Figures 1, S1, and S5) that may have formed within a shallow (<1 km) ocean: Lomonosov crater located at 64.9°N, 9.2°W ($D = 120$ km); Micoud located at 50.9°N, 343.7°E ($D = 50$ km); and an unnamed crater #2 located at 64°N, 349°W ($D = 42$ km). These craters were identified based on their locations and apparent age

and state of degradation, relative to the proposed shorelines (Figure S1). These craters are characterized by degraded rims, partially filled interiors, and lack clear ejecta blankets. Of these three craters, Lomonosov appears to be the best candidate source crater because its modeled inundation and backwash areas best match the mapped distribution of the TT (Costard et al., 2017).

The present study is a logical progression of our previously published work (Costard et al., 2017) which concluded that the TT unit originated from one or more impact-generated tsunamis. In the present study, we consider a variety of potential source craters for these tsunamis. The objectives of this work are to (1) study several complex impact craters in the northern plains of Mars by determining their ages and comparing their morphology with that of known marine impacts on Earth and (2) discuss the consistency of a potential marine origin of these Martian craters with the current evidence for a Late Hesperian/Early Amazonian northern ocean. To gain a better understanding of the dynamics of marine crater formation, a more detailed discussion of the main geological and morphological characteristics of terrestrial marine impacts follows.

1.2. Tsunami Generation by Marine Impacts on Earth

The ability of terrestrial marine impacts to generate tsunamis capable of leaving recognizable long-term traces on ocean shores has been extensively discussed (see review in Wünnemann et al., 2007). Considering the main physical processes of impact tsunami generation, the magnitude of the tsunami boils down to two main factors: (a) the size and proximity of the impact and (b) the rate at which the wave's energy decays with distance. A marine impact generates tsunamis in two principal ways: (1) by the displacement of water during the excavation phase, as the rim of the transient cavity propagates outward (i.e., “rim-wave tsunami”) and (2) by the in-rush and rebound of water—forming a second tsunami (i.e., the “collapse wave tsunami”)—following the collapse of the transient cavity (Wünnemann et al., 2007). The height of a rim wave tsunami may be very high near the origin of the impact (e.g., 2 km for the Lockne impact in central Sweden; Shuvalov et al., 2005), but will soon break and dissipate most of its energy relatively close to the impact site (Wünnemann et al., 2007).

In contrast, the subsequent collapse wave tsunami will generate a wave with a longer wavelength that can travel greater distances. Thus, the collapse wave tsunami is considered to be a greater hazard than the rim wave tsunami, despite its often smaller initial amplitude (Wünnemann et al., 2007). However, for a collapsing wave tsunami to form, the relative water depth at the location of the impact event must be very deep. Of the known marine impact craters on Earth that have been numerically simulated, none are known to have generated a collapse wave tsunami. The Lockne impact had the deepest relative target water depth (i.e., equal to the projectile diameter; Lindström et al., 2005; Ormö et al., 2007, 2010; Shuvalov et al., 2005). Still, the target water depth was not great enough to allow the collapse wave to overcome the ongoing water resurge over the crater rim area (Lindström et al., 2005; Ormö et al., 2010; Shuvalov et al., 2005). The same is likely true of all the other known impacts that occurred at shallow (relative to the projectile diameter) water depths.

There are a few craters on Earth that appear to be associated with distal tsunami deposits—for instance, the Rochechouart crater (Schmieder et al., 2010), the Alamo impact site (no preserved crater; e.g., Warme & Kuehner, 1998), the Kaluga crater (Dypvik et al., 2004), and the Tookoonooka crater (Bron, 2009). The largest known marine impact crater on Earth is the 150-km-diameter Chicxulub crater, buried deep beneath the coast of the Yucatan Peninsula in Mexico (e.g., Smit, 1999). Its age corresponds to the Cretaceous–Paleogene boundary (K–Pg boundary), 66 million years ago. The impact devastated the Gulf of Mexico region with a shock wave and air blast that radiated across the ocean. It generated substantial tsunami deposits and landforms in many areas around the Gulf of Mexico and the Caribbean, up to several hundred kilometers from the impact site. However, much of these tsunami effects were likely generated by the secondary collapse of the submarine shelf (i.e., the Campeche escarpment) due to seismic shaking from the impact (Smit, 1999). Wave heights greater than 200 m with subsequent backwash could have spanned the Gulf of Mexico (Matsui et al., 2002). The tsunami waves propagated more than 100 km inland into the main embayments of the Gulf of Mexico (Bourgeois et al., 1988) with subsequent deposition of sediments several meters thick. The sedimentary characteristics of the Chicxulub tsunami deposits can be observed along the Cretaceous–Palaeogene (K–Pg) boundary in the La Popa basin, Mexico. There, distal impact ejecta beds include some typical erosion and deposition features from violent ejecta-rich hyperconcentrated density flows caused by tsunami waves (Schulte et al., 2011). The deposits from subsequent tsunami backwash

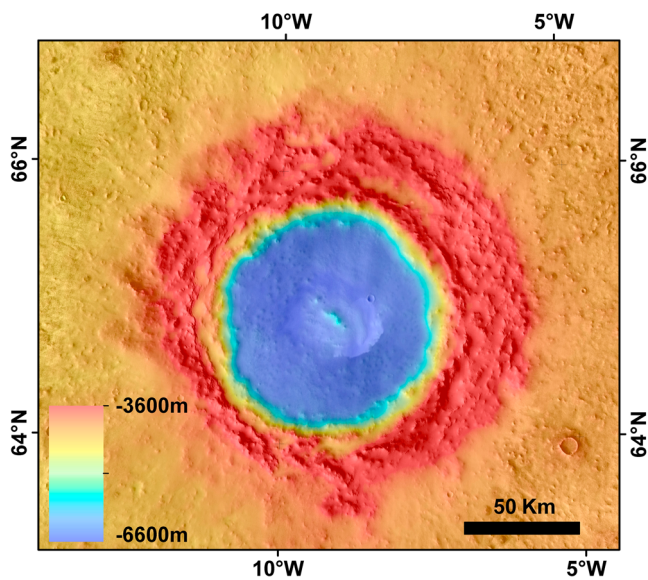


Figure 2. Topography of Lomonosov crater (Mars Orbiter Laser Altimeter digital elevation background). Courtesy of NASA/JPL/USGS.

surges show an erosive base with multiple-graded bedding structures. Mega-tsunami deposits initiated by the Chicxulub impact event are also commonly observed along the Mississippi Embayment (Campbell et al., 2008; King & Petruny, 2007) and were formed by the reworking of hot ejecta (Spherule beds) deposited soon after the impact (Clayton formation).

1.3. Geomorphological Signatures of Marine Impact Craters

Detailed geological, geophysical, experimental, and numerical investigations of marine impact craters on Earth have helped to constrain the marine impact process and allow estimates of the resulting crater morphology (e.g., see review by Ormö & Lindström, 2000). These studies reveal that the crater morphology, especially that of the rim, is affected by the marine target setting during both the crater excavation and modification stages. The effects depend primarily on the relative depth of the water (e.g., Lindström et al., 2005). For shallow water depths, the crater morphology closely resembles that of an impact on land (e.g., Ormö & Lindström, 2000) which are the conditions expected for the three candidate marine impact craters we have identified in the northern plains of Mars (Costard et al., 2017). According to Gault and Sonett (1982), at water depths equal the projectile diameter, the crater may develop a concentric

morphology with a smaller, nested crater inside a shallow, somewhat wider outer crater. The nested crater rim in these craters may be relatively low due to poor or absent structural uplift of the target rocks below the rim, while the part of the rim formed by ejected material may be broader than that produced by a similarly sized impact on land (e.g., Ormö & Lindström, 2000). This effect is particularly evident at the Lockne crater marine impact in Sweden (e.g., Lindström et al., 2005).

Conversely, the most conspicuous geomorphological features of a marine impact crater are the “resurge” gullies formed by inward flowing water during the collapse of the transient cavity (e.g., Dalwigk & Ormö, 2001; Ormö et al., 2007). Nevertheless, as a likely consequence of the poor preservation state of most terrestrial marine impact craters, few examples of such gullies have been reported (see review by Ormö & Lindström, 2000).

Although morphological features may give a strong indication of a marine impact crater, only the identification of resurge deposits in the crater infill as well as an unchanged marine facies of stratigraphically coeval sediments immediately below and above the impact can provide unambiguous confirmation (Ormö et al., 2002). Such confirmation is not currently possible for Martian craters.

In the next few sections, we will examine all of these morphometric criteria in relation to the potential marine impact craters we have identified in the northern plains of Mars and their consistency with the inferred geographic distribution and depth of a putative northern ocean.

2. Methods

Mars Orbiter Laser Altimeter (MOLA) gridded global digital elevation data were used for regional topographic analysis (463 m/pixel) while detailed local topographic considerations were obtained through MOLA PEDR laser shot analysis (vertical uncertainty of about ~1 m, horizontal precision ~100 m, with distance between individual shots on average 300 m; Smith et al., 2001). The topographic analysis has been performed by using the MOLA gridded global digital elevation data (463 m/pixel; Ferguson et al., 2018). The images (Figures 2 and 3) and the DEM were processed, calibrated, and georeferenced using the USGS Integrated Software for Imagers and Spectrometers (ISIS 3; Anderson et al., 2004).

We conducted an analysis of the width and volume of different crater rims for a number of different northern plains impact craters (Figures 1, 4, and S3–S5). The contour lines and rim height for each crater were calculated from the MOLA DEM. For the rim volume calculation, the base height was defined as the elevation where the rim begins (Lomonosov at $-4,700$ m, Micoud crater at $-4,000$ m, unnamed crater #2 at $-4,600$ m). The area of each crater was then divided into four quadrangles with two different orientations for better statistical analysis.

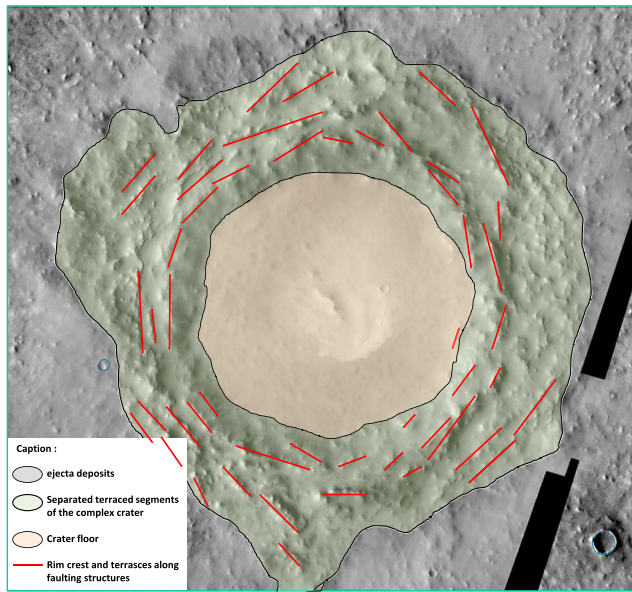


Figure 3. Geologic map of the Lomonosov complex impact crater. The rim shows some structural alignments and troughs consistent with typical structural terraces of complex crater rims. These localized rim collapse are potentially the cause of the infilling of the water from the surrounding sea just after the rim collapse. Courtesy of NASA/JPL/USGS.

In order to characterize the morphology of 10 complex impact craters in the northern plains (Figure 1), our analysis is based on the “standard” geometry of a complex crater rim with some terracing, using the methodology proposed by Sturm et al. (2016) to calculate ejecta thickness and structural uplift. Our measurements of rim height and ejecta thickness were made for craters larger than 40 km. According to Sturm et al. (2016), the ejecta-boundary contacts along the crater walls can be identified by analyzing the change in slope angle between the resistant uplifted bedrock and the overlapping friable ejecta blanket.

Sturm et al. (2016) calculated the relation between the radius of Martian complex impact craters and their associated structural rim uplift and ejecta thickness. These two parameters generally increase with increasing crater radius. They follow a power law and have been defined empirically for complex impact craters with diameter lower than 50 km. If we assume that these power laws can be applied for complex craters up to 120 km in diameter, we can compare the ideal morphometry of a crater of this size with its actual morphometry. Thus, we measured the structural rim uplift and the ejecta thickness for a variety of different craters (Figure 5) and considered whether these characteristics were consistent with a marine impact into an ocean with a depth of <1 km.

We dated the Lomonosov and TT units by the application of standard crater counting techniques (Figure 6). The TT unit covers an area of ~44,000 km² that includes 81 craters >1 km in diameter. The crater size-frequency distribution (CSFD) measured on Lomonosov was based on craters with diameters >350 m for its crater floor and craters with diameters >1 km for its ejecta blanket. For the CSFD measured on the ejecta blanket, an isochron (Hartmann, 2005) was fitted between 2- and 14-km-diameter bins. All crater counting was performed using the CraterTools module (Kneissl et al., 2011), while isochron fitting was done using CraterStats (Michael, 2013; Michael & Neukum, 2010)

diameters >350 m for its crater floor and craters with diameters >1 km for its ejecta blanket. For the CSFD measured on the ejecta blanket, an isochron (Hartmann, 2005) was fitted between 2- and 14-km-diameter bins. All crater counting was performed using the CraterTools module (Kneissl et al., 2011), while isochron fitting was done using CraterStats (Michael, 2013; Michael & Neukum, 2010)

3. Morphometric Analysis of Northern Complex Impact Craters on Mars

We conducted a comparative analysis of the average width of crater rims (normalized to the crater diameter) for the 10 complex craters (with diameter wider than 42 km, see Table 1) that were included in our study

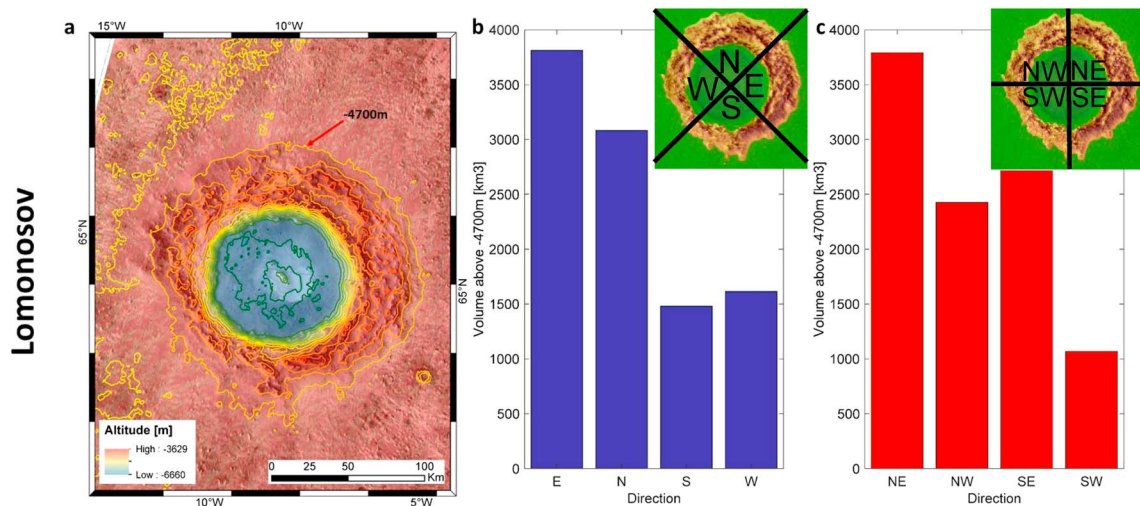


Figure 4. Volume calculation of Lomonosov’s rims from the base elevation of –4,700 m. (a) Topographic map of Lomonosov crater. Contour lines have been calculated from MOLA DTM (displayed as the background with THEMIS imagery in transparency) and displayed with a 250-m interval. (b) Rim volume calculation above the elevation –4,700 m according to four directions (see thumbnail). (c) The volume calculation is the same but the four quadrangles have been rotated 45°. The SW part of the rim appears to be underrepresented compared to the other parts of the crater rim.

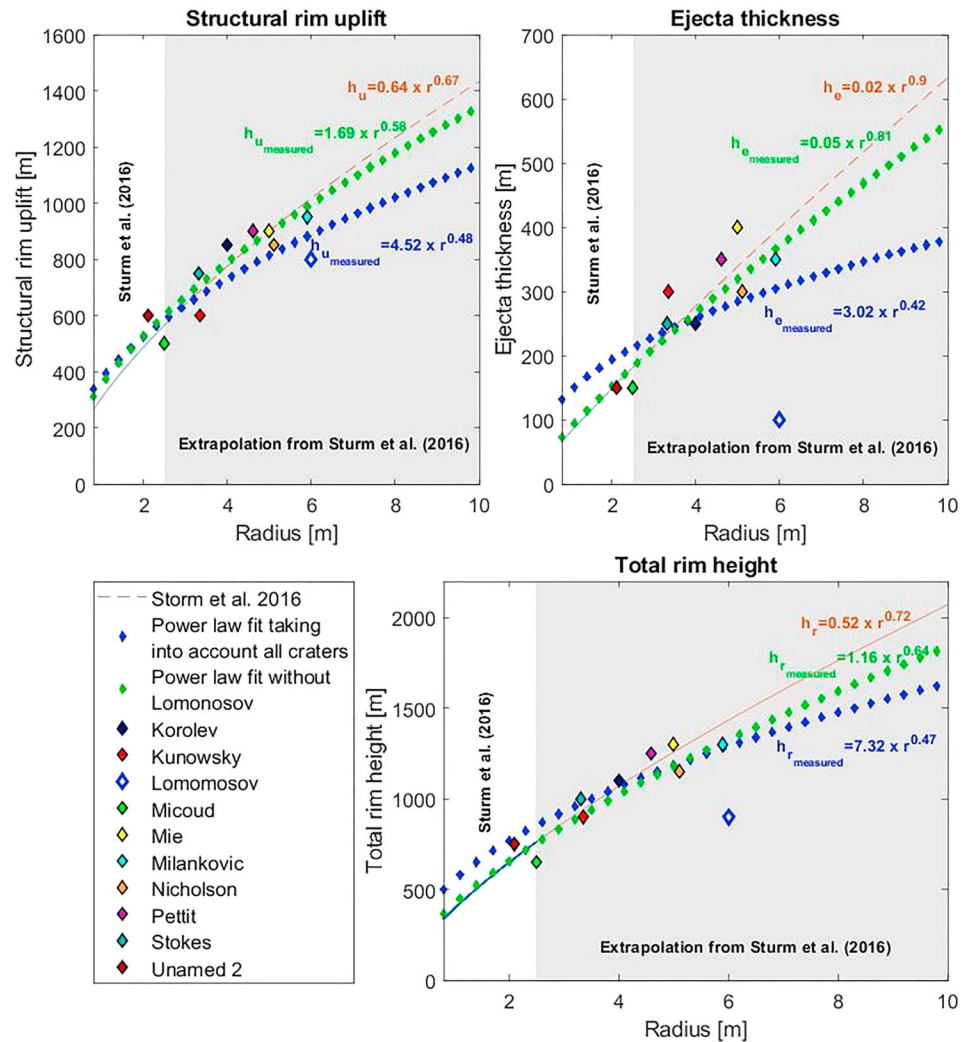


Figure 5. The relationship between the rim structural uplift, ejecta thickness, and total rim height versus crater radius for 10 large impact craters (with diameters between 42 and 120 km) located in the northern plains compared with the empirical relationship determined by Sturm et al. (2016) for craters smaller than 50 km in diameter (in orange). For each plot, two power laws have been fitted: in blue, by taking into account all impact craters, in green, by removing the Lomonosov crater from the fit. The structural rim uplift and the ejecta thickness are smaller for Lomonosov compared to other impact craters. When Lomonosov is taken into account for the fit (black diamonds), the fit is not a good match for the relationship found by Sturm et al. (2016). Conversely, a fit taking into account all other craters without Lomonosov (red diamond) produces a fit closer to this empirical law.

(Figures 1 and S5). The crater rim versus crater diameter ratio is between 0.14 to 0.15 for nine of the craters, but Lomonosov exhibits a notably wider crater rim. This is a ratio >0.18 , which is a much higher ratio than the similarly sized Milankovic crater (whose ratio is 0.15). Lomonosov's crater rim also exhibits some interesting asymmetries in plan view, as evident in the MOLA topographic data (Figure 4). The volume of the S and W part appears to be significantly smaller, by a factor of 2, compared to the other parts of the crater rim (Figure 4). We have performed the same detailed volume calculations for our two other marine impact candidates following Costard et al. (2017) (Figure S1): Micoud ($D = 50$ km, rim width ≈ 6 km, rim height ≈ 500 m) and the unnamed crater #2 ($D = 42$ km, rim width ≈ 5 km, rim height ≈ 500 m). However, unlike Lomonosov, their rims are relatively symmetric in their volume distribution (Figures S3 and S4).

We also conducted a morphometric analysis of the relation between the structural rim uplift, ejecta thickness, and total rim height. Our results are presented in Figure 5 and show a strong deviation between

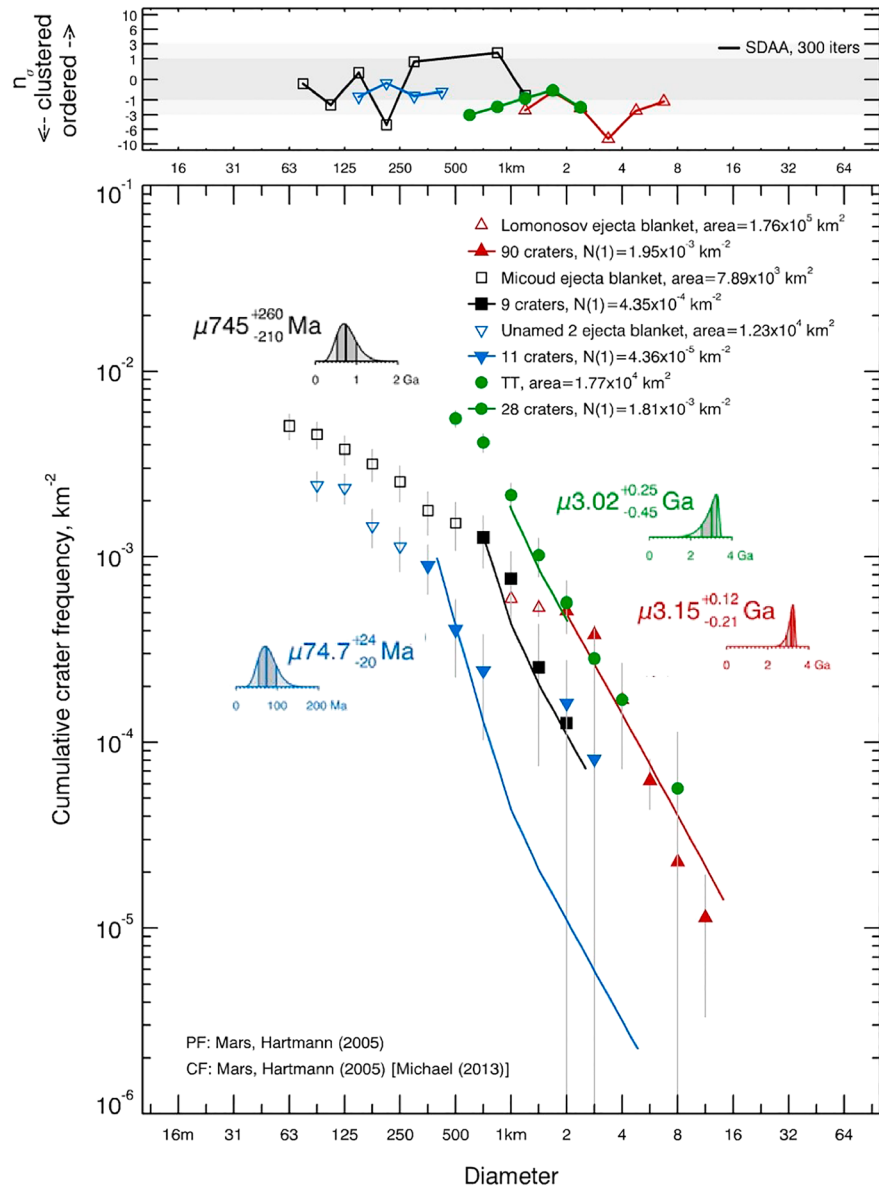


Figure 6. Crater size-frequency distribution (CSFD) of the three crater candidates and comparison with CSFD of the thumbprint terrains (TT), according to Hartmann's (2005) isochrons. Lomonosov crater is the only one to exhibit a CSFD as close to that of TT unit.

Lomonosov's theoretical structural rim uplift and ejecta thickness, and its measured values based on the MOLA data. The measured structural rim uplift is 20% less than its theoretical value, and the ejecta thickness is 75% less. Lomonosov's total rim height is therefore about half what it should be according to Sturm et al. (2016). Finally, our analysis points to an unusual morphometry of Lomonosov in comparison to the other northern craters. The comparative analysis of the width of the crater rims (normalized to the crater diameter; Figure 1) for these similarly sized northern impact craters demonstrates that Lomonosov's geometry is distinct from the others with its relatively broad and low crater rim. Fresh complex craters on the Moon generally exhibit greater topographic variability than simple lunar craters (Kalynn et al., 2013). And while a comparison between the observed dimensions of Martian craters with the power law relations of Sturm et al. (2016) suggests that there is an increase in topographic variability with increasing crater radius, Figure 1 clearly shows that the normalized rim width of Lomonosov is

significantly greater than that of the three other craters having diameters >100 km (Mie, Nicholson, and Milankovic), which generally follow the same trend as smaller impact craters.

4. Lomonosov Crater: A Potential Marine Impact Crater

Lomonosov is an ~120-km-diameter impact crater characterized by a relatively shallow, but broad, rim and a relatively small central peak area (Figure 2). At the ejecta's outer limit, its surface roughness, as determined from an analysis of MOLA data (Kreslavsky & Head, 2000), is notably smoother at 2.4-km scales than its surroundings (Figure S2). The ejected impact material is widely distributed, extending over four crater radii, and the ejecta blanket is very thin. In comparison, the rim is associated with a higher roughness (at 19.2-km scale; Figure S2).

Lomonosov crater shows a subdued rim suggesting that something caused a deviation from the expected crater geometry, either during the cratering process, or by later modification due to erosion, or both. We propose that this subdued appearance was due to the presence of an ocean of liquid water at the time of the impact.

According to our previous simulations, the ocean shoreline would have been at $-3,860$ m so if the seafloor at Lomonosov was at $-4,700$ m, the ocean depth would have been about 840 m. From the model, the estimated projectile diameter was about 15–20 km, resulting in a transient cavity diameter of 70 km and a final crater diameter of 120 km. The total rim height of Lomonosov is about 900 m—so approximately equivalent to the depth of the ocean. According to Gault and Sonett (1982) and Hoffman et al. (2005), for $(d/h) > 1.0$ (d : crater diameter, h : water depth), the presence of a water column is negligible in terms of its effect on the cratering process. So Lomonosov would correspond to a shallow water impact.

The rim shows separate terraced segments with linear rim crests and many gaps through the rims (Figure 3). Lomonosov has a relatively broader rim, a lower structural uplift, ejecta thickness, and rim height than other comparable craters in the northern plains (e.g., Micoud, Korolev, and other craters >50 km in diameter). Taken together, these morphological characteristics are similar to those of marine impact craters on Earth, indicating a likely marine origin for Lomonosov (Table 2).

The distinct geometrical characteristics of Lomonosov could be the result of erosion/deposition activity after its formation. A radically different rheology of the impacted material is excluded as an explanation of Lomonosov's "anomaly" because all the other examined impact craters were formed in the same geological unit (northern plain unit, Vastitas Borealis Formation).

5. Crater Count Methods and Results

From our morphometric analysis, it appears that Lomonosov presents an unusual morphology, distinct from the other complex impact craters in the northern plains. We tested the consistency in age of Lomonosov, and the two other potential candidate source craters identified in our previous numerical study (Costard et al., 2017), with the age of the inferred tsunami deposits (TT) identified along the dichotomy boundary, north

Table 2

A comparison of the Geomorphological and Main Sedimentological Characteristics of Terrestrial Marine-Target Impact Craters Versus Lomonosov

Marine impacts (Earth)	Lomonosov (Mars)
Concentric morphology ("inverted sombrero") with deep nested crater surrounded by shallow outer crater	?
Shallow rim due to relatively low structural uplift	X
Broad rim due to relatively more extensive ejecta flaps	X
Gaps through the flaps due to tangential stresses (rip-apart) during excavation and/or resurge flow	X
Poorly developed ejecta blanket due to ejecta landing in water and subsequent resurge erosion. At very shallow water depth fluidized ejecta (i.e., lobate ejecta morphologies) may form	X
Resurge gullies (often in connection with the rip-apart gaps, but may form more extensive erosional features beyond the crater rim)	?
Resurge deposits (Hard to discern in remote sensing, but submarine fan or delta features could evolve. They must be linked to the crater formation and not later fluvial processes.)	?
Continuous marine sedimentation (Can only be seen in outcrop or drill core)	?

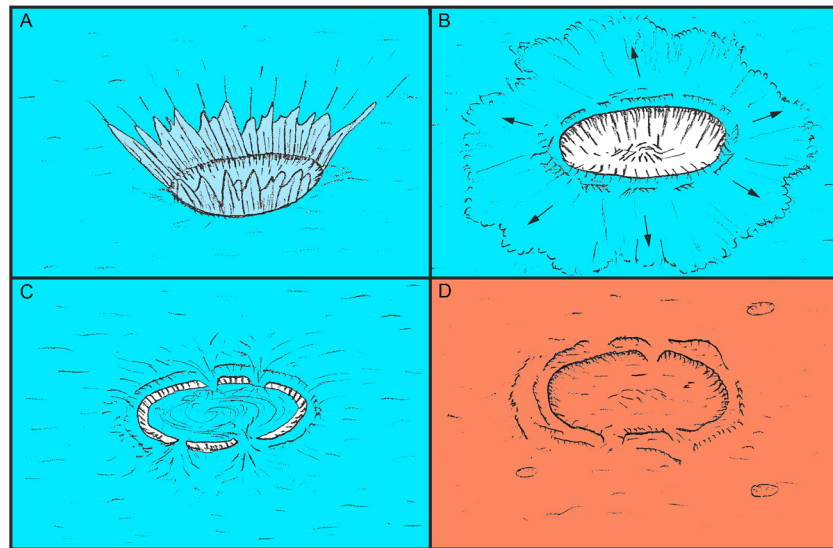


Figure 7. Proposed formation of the Lomonosov marine impact crater on Mars. (a) Formation of the transient cavity in a shallow ocean, development of the ejecta curtain. (b) Propagation of the rim-wave tsunami. (c) Localized rim collapse can cause openings for the surrounding sea with crater infilling. (d) Present morphology of the crater after withdrawal of the ocean.

of Arabia Terra. We measured the CSFD of the TT unit, and the ejecta blankets of our different source crater candidates. The CSFD of the TT unit indicates an Early Amazonian (~ 3 Ga) age (Figure 6), while Micoud and the unnamed crater #2 both show a Late Amazonian age—the latter two being clearly distinct from the age of lobate tsunami deposits (TT unit). These results indicate that Lomonosov was formed during the transition between the Late Hesperian and the Early Amazonian at about $\sim 3.15^{+0.12}_{-0.21}$ Ga (Figure 6). There is a clear agreement between the age of Lomonosov and the age of the inferred tsunami lobate deposits (TT unit), dated at $\sim 3.02^{+0.25}_{-0.45}$ Ga (Figure 6)—consistent with the belief that Lomonosov was the source crater that generated the tsunami that deposited the TT lobes (Costard et al., 2017; Rodriguez et al., 2016).

The presence of small craters on Lomonosov's ejecta suggests that they date the time by which the northern ocean had disappeared. The shape of the CSFD measured on the ejecta blankets of the three candidate source craters does not show any inflection in the crater population >2 km in diameter (Figure 6), which would indicate a postimpact resurfacing episode. Because the CSFD fits the production function for the 2-km bin, it means that any resurfacing activity that occurred in this area since the emplacement of Lomonosov is not sufficient to obliterate 2-km craters. Thus, we conclude that any resurfacing processes that were at work here were not sufficient to significantly alter the morphology of Lomonosov.

We therefore conclude that the likely explanation for the differences between the theoretical and actual rim uplift and ejecta thickness of Lomonosov is not due to its 3 Gyr of erosion history but to the dynamic processes affecting its morphology during its emplacement.

6. Discussion

Based on our morphologic and morphometric analysis, we believe that Lomonosov was formed by a marine impact and is the most probable source of the tsunami that created the lobate deposits of the TT. Our morphometric approach shows that Lomonosov exhibits an unusually broad and low concentric rim at an elevation equal to that inferred for the past ocean level, which would have resulted in the infilling of the crater. Our previous numerical models (Costard et al., 2017) indicate that the formation of Lomonosov would have required an impact into a shallow ocean (≤ 1 km deep) which supports our conclusions.

In summary, Figure 7 shows the principal stages, including (1) the impactor's penetration into the target and the development of the transient cavity (Figure 7a) and (2) the generation and propagation of tsunami waves (Figure 7b). The broad and low rim would be the result of erosion from the infilling of the crater after the collapse of the transient cavity (Figure 7c). The forceful erosion of the crater rim by the in-rushing water

may have resulted in the formation of radial resurge gullies. Unfortunately, we did not observe evidence of any such features associated with Lomonosov, possibly due to the lack of high-resolution coverage in that area but perhaps due to the presence of the more recent latitude-dependent mantle deposit. As noted by Ormó et al. (2004), in the absence of evidence of diagnostic resurge deposits and a continuous episode of marine sedimentation before and after the impact, recognition of a marine impact crater must be based on the identification of possible morphological features such as crater concentricity, low and broad rim, and radial (resurge) gullies, as well as other evidence supporting a marine target setting. Interestingly, we can observe many gaps through Lomonosov's rims (Figures 2 and 3) that show some analogy to potential resurge valleys of terrestrial marine impact craters. The other morphometric criteria are a crater's concentricity and its low and broad rim, which are clearly characteristics of the morphology of Lomonosov (see Table 2).

The relatively poor development of the central peak and the broad rim of Lomonosov are best explained by a target layering consisting of relatively thick and poorly consolidated marine sediments (Hopkins et al., 2019), covering a more rigid basement. In such a case, terrestrial investigations clearly show that extensive collapse of the sedimentary strata can expand the size of the crater to several times the diameter of the initial crater in the basement. This could be the case with the Vastitas Borealis Formation in the northern plains. The strong slumping of sediments may both cut and cover the basement crater rim. This is especially evident at the Chesapeake Bay Impact Structure in the United States (e.g., Collins & Wünnemann, 2005; Horton et al., 2005), and has been suggested as an explanation for the morphology of craters on Mars that are believed to have formed in a volatile-rich, albeit not necessarily marine, environment (Horton et al., 2006).

These results also have important implications for understanding the stability and duration of a late northern ocean on Mars. The good agreement between the crater count age of the Lomonosov crater floor and ejecta and the TT unit implies a northern ocean during the Amazonian/Hesperian transition. This is also the timing of peak outflow channel activity (Warner et al., 2009), and is thus consistent with the presence of a transient northern ocean ~3.2 Ga (Clifford & Parker, 2001).

Acknowledgments

The authors acknowledge the HRSC Team of the German Aerospace Center (DLR) Berlin, who provided map projected HRSC image data. The topographic analysis has been performed by using the blended global-scale DEM from MOLA and HRSC data (https://astrogeology.usgs.gov/search/map/Mars/Topography/HRSC_MOLA_Blend/Mars_HRSC_MOLA_BlendDEM_Global_200mp_v2). The project is financed by the Programme National de Planétologie (PNP) of Institut National des Sciences de l'Univers (CNRS-INSU), the Centre National d'Etudes Spatiales (CNES), and National Aeronautics and Space Administration (NASA). The work by A. Lagain was partially supported by Australian Research Council (FT170100024) and Curtin University and the Domaine d'Intérêt Majeur pour l'Astrophysique et les Conditions de l'Apparition de la Vie (DIM ACAV) from the Région Île de France. The work by J. Ormó was partially supported by grants ESP2014-59789-P, ESP2015-65712-C5-1-R, and ESP2017-87676-C5-1-R from the Spanish Ministry of Economy and Competitiveness and Fondo Europeo de Desarrollo Regional. We acknowledge A. Barrett and an anonymous reviewer for their constructive reviews. We acknowledge the comments of the Associate Editor Caleb Fassett.

7. Conclusion

Our previous work (Costard et al., 2017; Rodriguez et al., 2016) concluded that the most plausible explanation for the origin of the TT lobate deposits, with runups, found along the dichotomy boundary, especially in Arabia Terra, was tsunami deposits. The Late Hesperian/Early Amazonian Lomonosov crater is the best candidate for a marine impact crater discovered outside of Earth. Interestingly, this impact crater exhibits a volume anomaly with a broad and subdued concentric rim suggesting the collapse of the transient cavity under marine conditions. The likely marine origin of Lomonosov, and the correspondence in time with the TT unit (approximately 3 Ga), strongly suggests that Lomonosov was the source crater for the tsunami.

However, further investigations are still required to fully assess and validate the marine origin of the Lomonosov crater. The southern rim asymmetry might reveal new details with higher-resolution data sets. Furthermore, to refine the diagnostic morphologic criteria, we plan to conduct numerous high-resolution impact simulations to match the fine-scale geomorphology not just in bed form patterns but also in mass distributions.

The evidence for the occurrence of these tsunamis supports the belief that an ocean occupied the northern plains of Mars as recently as ~3 billion years ago. This has implications for the total inventory of water on Mars, how it evolved with time, and the potential for the origin and survival of life on the Red Planet. In the near future, we will investigate some other sites where this method could be used to identify marine craters. If there was a Late Hesperian/Early Amazonian ocean on Mars, then the presence of other craters with similar properties would be expected. Thus, their presence or absence could provide further evidence regarding the existence of a northern ocean.

References

- Anderson, J. A., Sides, S. C., Soltész, D. L., Sucharski, T. L., & Becker, K. J. (2004). Modernization of the Integrated Software for Imagers and Spectrometers 35th Lunar and Planetary Institute, Science Conference Abstracts, 2039.
- Baker, V. R., Strom, R. G., Gulick, V. C., Kargel, J. S., Komatsu, G., & Kale, V. S. (1991). Ancient oceans, ice sheets and the hydrological cycle on Mars. *Nature*, 352(6336), 589–594. <https://doi.org/10.1038/352589a0>
- Bourgeois, J. T. A., Hansen, P., Wiberg, P. L., & Kauffman, E. G. (1988). A tsunami deposit at the Cretaceous-Tertiary boundary in Texas. *Science*, 241, 567–570.

- Bron, K. (2009). The Tookoonooka tsunami sequence: Evidence for marine impact in Australia's Lower Cretaceous. (abstract #2560). 40th Lunar and Planetary Science Conference, CD-Rom.
- Campbell, C. E., Oboh-Ikuenobe, F. E., & Eifert, T. L. (2008). Megatsunami deposit in Cretaceous-Paleogene boundary interval of south-eastern Missouri. *The Geological Society of America Special Paper*, 437, 189–198. [https://doi.org/10.1130/2008.2437\(11\)](https://doi.org/10.1130/2008.2437(11))
- Carr, M. H., & Head, J. W. III. (2003). Oceans on Mars: An assessment of the observational evidence and possible fate. *Journal of Geophysical Research*, 108(E5), 5042. <https://doi.org/10.1029/2002JE001963>
- Citron, R. I., Manga, M., & Hemingway, D. J. (2018). Timing of oceans from shoreline deformation. *Nature*, 555(7698), 643–646. <https://doi.org/10.1038/nature26144>
- Clifford, S. M., & Parker, T. J. (2001). The evolution of the Martian hydrosphere: Implications for the fate of a primordial ocean and the current state of the Northern Plains. *Icarus*, 154(1), 40–79. <https://doi.org/10.1006/icar.2001.6671>
- Collins, G. S., & Wünnemann, K. (2005). How big was the Chesapeake Bay impact? Insight from numerical modeling. *Geology*, 33(12), 925–928. <https://doi.org/10.1130/G21854.1>
- Costard, F., Séjourné, A., Kelfoun, K., Clifford, S., Lavigne, F., Di Pxierto, I., & Bouley, S. (2017). Modeling tsunami propagation and the emplacement of thumbprint terrain in an early Mars ocean. *Journal of Geophysical Research: Planets*, 122, 633–649. <https://doi.org/10.1002/2016JE005230>
- Dalwigk, V., & Ormö, J. (2001). Formation of resurge gullies at impacts at sea: The Lockne crater, Sweden. *Meteoritics & Planetary Science*, 36(3), 359–369. <https://doi.org/10.1111/j.1945-5100.2001.tb01879.x>
- Dypvik, H., Mørk, A., Smelror, M., Sandbakken, P., Tsikalas, F., Vigran, J. O., et al. (2004). Impact breccia and ejecta from the Mjølner crater in the Barents Sea—The Ragnarok formation and Sindre Bed. *Norsk Geologisk Tidsskrift*, 84, 143–167. <https://doi.org/10.2204/iodp.sd.6.09.2008>
- Ferguson, R. L., Hare, T. M., Laura, J. (2018). HRSC and MOLA Blended Digital Elevation Model at 200 m v2, Astrogeology PDS Annex, U.S. Geological Survey. Retrieved from http://bit.ly/HRSC_MOLA_Blend_v0
- Gault, D. E., & Sonett, C. P. (1982). Laboratory simulation of pelagic asteroidal impact: Atmospheric injection, benthic topography, and the surface wave radiation field. In L. T. Silver & P. H. Schultz (Eds.), *Geological implications of impacts of large asteroids and comets on the Earth, Special Paper* (Vol. 190, pp. 69–92). Geological Society of America.
- Ghatan, G. J., & Zimbelman, J. R. (2006). Paucity of candidate coastal constructional landforms along proposed shorelines on Mars: Implications for a northern lowlands-filling ocean. *Icarus*, 185(1), 171–196. <https://doi.org/10.1016/j.icarus.2006.06.007>
- Guidat, G., Pochat, S., Bourgeois, O., & Souček, O. (2015). Landform assemblage in Isidis Planitia, Mars: Evidence for a 3 Ga old polythermal ice sheet. *Earth and Planetary Science Letters*, 411, 253–267. <https://doi.org/10.1016/j.epsl.2014.12.002>
- Hartmann, W. (2005). Martian cratering: Isochron refinement and the chronology of Mars. *Icarus*, 174(2), 294–320. <https://doi.org/10.1016/j.icarus.2004.11.023>
- Head, J. W., Mustard, J. F., Kreslavsky, M., Milliken, R. E., & Marchant, D. R. (2003). Recent ice ages on Mars. *Nature*, 426(6968), 797–802. <https://doi.org/10.1038/nature02114>
- Hoffmann, V., Rösler, W., Patzelt, A., Raeymaekers, B., & Van Espen, P. (2005). Characterization of a small crater-like structure in southeast Bavaria, Germany. *Meteoritics and Planetary Science*, 40, A129.
- Hopkins, R., Osinski, G. R., & Collins, G. S. (2019). Formation of complex craters in layered targets with material anisotropy. *Journal of Geophysical Research: Planets*, 124, 349–373. <https://doi.org/10.1029/2018JE005819>
- Horton J. W., Jr., Powars D. S., Gohn G. S., & Ormö J. (2005). Chesapeake Bay impact structure: Morphology, crater fill, and relevance for impact processes on Mars (abstract #3024). Workshop on the Role of Volatiles and Atmospheres on Martian Impact Craters (pp. 57–58).
- Horton, J. W. Jr., Powars, D. S., Ormö, J., & Gohn, G. S. (2006). Chesapeake Bay impact structure: Morphology, crater fill, and relevance for impact structures on Mars. *Meteoritics & Planetary Science*, 41(10), 1613–1624. <https://doi.org/10.1111/j.1945-5100.2006.tb00439.x>
- Iijima, Y., Goto, K., Minoura, K., Komatsu, G., & Imamura, F. (2014). Hydrodynamics of impact-induced tsunami over the Martian ocean. *Planetary and Space Science*, 95, 33–44. <https://doi.org/10.1016/j.pss.2013.09.014>
- Kalynn, J., Johnson, C. L., Osinski, G. R., & Barnouin, O. (2013). Topographic characterization of lunar complex craters. *Geophysical Research Letters*, 40, 38–42. <https://doi.org/10.1029/2012GL053608>
- King, D. T., & Petruny, L. W. (2007). Impact spherule-bearing, Cretaceous-Tertiary boundary sand body, Shell Creek stratigraphic section, Alabama, USA. *Special Paper of the Geological Society of America*, 437, 179–187. [https://doi.org/10.1130/2008.2437\(10\)](https://doi.org/10.1130/2008.2437(10))
- Kneissl, T., Van Gasselt, S., & Neukum, G. (2011). Map-projection-independent crater size-frequency determination in GIS environments—New software tool for ArcGIS. *Planetary and Space Science*, 59(11–12), 1243–1254. <https://doi.org/10.1016/j.pss.2010.03.015>
- Kreslavsky, M. A., & Head, J. W. (2000). Kilometer-scale roughness of Mars' surface: Results from MOLA data analysis. *Journal of Geophysical Research*, 105(E11), 26,695–26,711. <https://doi.org/10.1029/2000JE001259>
- Kreslavsky, M. A., & Head, J. W. (2002). Mars: Nature and evolution of young latitude-dependent water-rich mantle. *Geophysical Research Letters*, 29(15), 1719. <https://doi.org/10.1029/2002GL015392>
- Lindström, M., Shuvalov, V., & Boris, I. (2005). Lockne Crater as a result of marine-target oblique impact. *Planetary and Space Science*, 53(8), 803–815. <https://doi.org/10.1016/j.pss.2005.02.005>
- Lucchitta, B. K. (1981). Mars and Earth: Comparison of cold-climate features. *Icarus*, 45(2), 264–303. [https://doi.org/10.1016/0019-1035\(81\)90035-X](https://doi.org/10.1016/0019-1035(81)90035-X)
- Mahaney, W. C., Dohm, J. M., Costa, P., & Krinsley, D. H. (2010). Tsunamis on Mars: Earth analogues of projected Martian sediment. *Planetary and Space Science*, 58(14–15), 1823–1831. <https://doi.org/10.1016/j.pss.2010.08.010>
- Malin, C., & Edgett, K. (1999). Oceans or seas in the Martian northern lowlands: High-resolution imaging tests of proposed coastlines. *Geophysical Research Letters*, 26(19), 3049–3052. <https://doi.org/10.1029/1999GL002342>
- Matsui, T., Imamura, F., Tajika, E., Nakano, Y., & Fujisawa, Y. (2002). *Generation and propagation of a tsunami from the cretaceous-Tertiary impact event, Special paper* (Vol. 356, pp. 69–77). Geological Society of America.
- Matsui, T., Takamiya, I., Imamura, F., & Tajika, E. (2001). Tsunami generation and propagation in possible ancient ocean on Mars. In *Lunar and Planetary Science Conference XXXII. Abstract #1716* (Vol. 32, p. 1716). Houston, TX.
- Michael, G. G. (2013). Planetary surface dating from crater size–frequency distribution measurements: Multiple resurfacing episodes and differential isochron fitting. *Icarus*, 226(1), 885–890. <https://doi.org/10.1016/j.icarus.2013.07.004>
- Michael, G. G., & Neukum, G. (2010). Planetary surface dating from crater size-frequency distribution measurements: Partial resurfacing events and statistical age uncertainty. *Earth and Planetary Science Letters*, 294(3–4), 223–229. <https://doi.org/10.1016/j.epsl.2009.12.041>
- Mustard, J. F., Cooper, C. D., & Rifkin, M. K. (2001). Evidence for recent climate change on Mars from the identification of youthful near-surface ground ice. *Nature*, 412(6845), 411–414. <https://doi.org/10.1038/35086515>

- Ormö, J., Dohm, J. M., Ferris, J. C., Lepinette, A., & Fairén, A. G. (2004). Marine-target craters on Mars? An assessment study. *Meteoritics and Planetary Science*, 39(2), 333–346. <https://doi.org/10.1111/j.1945-5100.2004.tb00344.x>
- Ormö, J., & Lindström, M. (2000). When a cosmic impact strikes the seabed. *Geological Magazine*, 137(1), 67–80. <https://doi.org/10.1017/S001675680003538>
- Ormö, J., Lindström, M., Lepinette, A., Martínez-Frias, J., & Enrique, D. M. (2010). Cratering and modification of wet-target craters: Projectile impact experiments and field observations of the Lockne marine-target crater (Sweden). *Meteoritics & Planetary Science*, 41, 1605–1612. <https://doi.org/10.1111/j.1945-5100.2006.tb00438.x>
- Ormö, J., Shuvalov, V. V., & Lindström, M. (2002). Numerical modeling for target water depth estimation of marine-target impact craters. *Journal of Geophysical Research*, 107(E12), 3–1–3–9. <https://doi.org/10.1029/2002JE001865>
- Ormö, J., Sturkell, E., & Lindström, M. (2007). Sedimentological analysis of resurge deposits at the Lockne and Tvären craters: Clues to flow dynamics. *Meteoritics and Planetary Science*, 42(11), 1929–1943. <https://doi.org/10.1111/j.1945-5100.2007.tb00551.x>
- Parker, T. J., Gorsline, D. S., Saunders, R. S., Pieri, D. C., & Schneeberger, D. M. (1993). Coastal geomorphology of the martian northern plains. *Journal of Geophysical Research*, 98(E6), 11,061–11,078. <https://doi.org/10.1029/93JE00618>
- Parker, T. J., Saunders, R. S., & Schneeberger, D. M. (1989). Transitional morphology in West Deuteronilus Mensae, Mars: Implications for modification of the Lowland/Upland boundary. *Icarus*, 82(1), 111–145. [https://doi.org/10.1016/0019-1035\(89\)90027-4](https://doi.org/10.1016/0019-1035(89)90027-4)
- Rodríguez, J. A., Fairén, A. G., Tanaka, K. L., Zarroca, M., Linares, R., Platz, T., et al. (2016). Tsunami waves extensively resurfaced the shorelines of an early Martian ocean. *Scientific Reports*, 6(1), 25106. <https://doi.org/10.1038/srep25106>
- Rodríguez, J. A. P., Gulick, V., Baker, V., Platz, T. H., Fairén, A. G., Yan, J., et al. (2014). Evidence for Middle Amazonian catastrophic flooding and glaciation on Mars. *Icarus*, 242, 202–210. <https://doi.org/10.1016/j.icarus.2014.06.008>
- Rodríguez, J. A. P., Platz, T. H., Gulick, V., Baker, V., Fairén, A. G., Kargel, J., et al. (2015). Did the outflow channels mostly form during the Amazonian Period? *Icarus*, 257, 387–395. <https://doi.org/10.1016/j.icarus.2015.04.024>
- Salvatore, M. R., & Christensen, P. R. (2014). Evidence for widespread aqueous sedimentation in the northern plains of Mars. *Geology*, 42(5), 423–426. <https://doi.org/10.1130/G35319.1>
- Schmieder, M., Buchner, E., Schwarz, W. H., Tieloff, M., & Lambert, P. (2010). A Rhaetian ⁴⁰Ar/³⁹Ar age for the Rochechouart impact structure (France) and implications for the latest Triassic sedimentary record. *Meteoritics and Planetary Science*, 45(8), 1225–1242. <https://doi.org/10.1111/j.1945-5100.2010.01070.x>
- Schulte, P., Smit, J., Deutsch, A., Salge, T., Friese, A., & Beichel, K. (2011). Tsunami backwash deposits with Chicxulub impact ejecta and dinosaur remains from the Cretaceous–Palaeogene boundary in the La Popa Basin, Mexico. *Sedimentology*, 59(3), 737–765. <https://doi.org/10.1111/j.1365-3091.2011.01274.x>
- Sholes, S. F., Montgomery, D., & Catling, D. C. (2019). Quantitative high-resolution re-examination of a hypothesized ocean shoreline in Cydonia Mensae on Mars. *Journal of Geophysical Research: Planets*, 124, 316–336. <https://doi.org/10.1029/2018JE005837>
- Shuvalov, V., Ormö, J., & Lindström, M. (2005). Hydrocode simulation of the Lockne marine-target impact event. In *Impact Tectonics* (pp. 405–422). Berlin, Heidelberg: Springer. <https://doi.org/10.1007/3-540-27548-7>
- Smit, J. (1999). The global stratigraphy of the Cretaceous–Tertiary boundary impact ejecta. *Annual Review of Earth and Planetary Sciences*, 27(1), 75–113. <https://doi.org/10.1146/annurev.earth.27.1.75>
- Smith, D. E., Zuber, M. T., Frey, H. V., Garvin, J. B., Head, J. W., Muhleman, D. O., et al. (2001). Mars Orbiter Laser Altimeter: Experiment summary after the first year of global mapping of Mars. *Journal of Geophysical Research, Planets*, 106(E10), 23,689–23,722. <https://doi.org/10.1029/2000JE001364>
- Sturm, S., Kenkmann, T., & Hergarten, S. (2016). Ejecta thickness and structural rim uplift measurements of Martian impact craters: Implications for the rim formation of complex impact craters. *Journal of Geophysical Research: Planets*, 121, 1026–1053. <https://doi.org/10.1002/2015je004959>
- Tanaka K. L., Skinner, J. A., Dohm, J. M., Irwin, R. P., Kolb, E. J., Fortezzo, C. M., et al. (2014). Geologic map of Mars: U.S. Geological Survey Scientific Investigations Map 3292, scale 1:20,000,000, pamphlet 43 p.
- Turbet, M., & Forget, F. (2019). The paradoxes of the Late Hesperian Mars ocean. *Scientific Reports*, 9(1), 5717. <https://doi.org/10.1038/s41598-019-42030-2>
- Villiers, G., King, D. T., & Marzen, L. J. (2010). A study of candidate marine target impact craters in Arabia Terra, Mars. *Meteoritics and Planetary Science*, 45(6), 947–964. <https://doi.org/10.1111/j.1945-5100.2010.01068.x>
- Warme, J., & Kuehner, H. C. (1998). Anatomy of an anomaly: The Devonian catastrophic Alamo impact breccia of southern Nevada. *International Geology Review*, 40(3), 189–216. <https://doi.org/10.1080/00206819809465206>
- Warner, N., Gupta, S., Muller, J. P., Kim, J. R., & Lin, S. Y. (2009). A refined chronology of catastrophic outflow events in Ares Vallis, Mars. *Earth and Planetary Science Letters*, 288(1–2), 58–69. <https://doi.org/10.1016/j.epsl.2009.09.008>
- Wordsworth, R. D. (2016). The climate of early Mars. *Annual Review of Earth and Planetary Sciences*, 44(1), 381–408. <https://doi.org/10.1146/annurev-earth-060115-012355>
- Wünnemann, K., Weiss, R., & Hofmann, K. (2007). Characteristics of oceanic impact-induced large water waves—Re-evaluation of the tsunami hazard. *Meteoritics and Planetary Science*, 42(11), 1893–1903. <https://doi.org/10.1111/j.1945-5100.2007.tb00548.x>